Correlating the Synthesis, Structure and Catalytic Performance of Pt-Re/TiO_2 for the Aqueous-Phase Hydrogenation of Carboxylic Acid Derivatives

*Moritz O. Haus[1], Alexander Meledin[2,3], Sebastian Leiting[4], Yannik Louven[1], Nico C. Roubicek[1], Sven Moos[1], Claudia Weidenthaler[4], Thomas E. Weirich[2] and Regina Palkovits[1,]**

[1] Lehrstuhl für Heterogene Katalyse und Technische Chemie, RWTH Aachen University, Worringerweg 2, DE-52074 Aachen.

[2] Gemeinschaftslabor für Elektronenmikroskopie, RWTH Aachen University, Ahornstraße 55, DE-52074, Aachen.

[3] Ernst Ruska-Centre for Microscopy and Spectroscopy with Electrons (ER-C), Forschungszentrum Jülich GmbH, DE-52428 Jülich

[4] Max-Planck-Institut für Kohlenforschung, Kaiser-Wilhelm-Platz 1, D-45470 Mülheim an der Ruhr.

*E-Mail: palkovits@itmc.rwth-aachen.de

ABSTRACT

Pt-Re bimetallic catalysts have many applications, ranging from catalytic reforming to the reduction of carboxylic acid derivatives. However, the exact role of Re in these systems has remained a matter of discussion, partly due to the plethora of suggested synthesis protocols and analysis conditions. This study presents an extensive comparison of such literature protocols and the resulting materials. In detail, characterization by N_2 physisorption, XRD, TPR, CO pulse chemisorption, CO-FTIR, STEM-EDX and *in-situ* XPS is combined with catalytic testing to yield synthesis-structure-activity correlations. Accordingly, the investigated catalysts share common features, such as Pt^0 nanoparticles (1-4 nm) decorated with partially reduced Re species (ReO_{x-y}). Remaining rhenium oxide is spread over the TiO_2 support and enhances Pt dispersion in sequential impregnation protocols. While differences in the number of active sites (Pt^0/ReO_{x-y}) mostly explain catalytic results, small variations in the extent of Re reduction and site composition cause additional modulations. The optimal bimetallic catalyst outperforms Ru/C (previous benchmark) in the reduction of *N*-(2-hydroxyethyl)succinimide, an important step in the production of a bio-based polyvinylpyrrolidone polymer.

KEYWORDS

Platinum, rhenium, hydrogenation, succinic acid, structure-activity, bimetallic catalyst, bifunctional, catalyst preparation.

1. Introduction

Pt-Re bimetallic catalysts have attracted substantial research attention for several decades, initially due to their application in catalytic reforming processes.[1] In this context, it has been noted that the choice of preparation procedure largely impacts on the catalytic properties of the final material. For example, Re deposition onto a parent Pt-catalyst by way of surface redox reactions (catalytic reduction = CR) has yielded superior reforming catalysts as compared to simple co-impregnation, which was ascribed to the proximity of Pt and Re species.[2] Moreover, Pt-Re interactions, which are indirectly evident from the enhanced reduction of Re in bimetallic catalysts,[3,4] were significantly affected by temperature treatments during catalyst synthesis.[5] Due to these variabilities, the detailed function and even the oxidation state of Re in reforming catalysts have remained a matter of much discussion.[1,4,6] The complex redox chemistry of Pt-Re, which includes the potential for alloy formation, has been another factor in this regard.[7-9]

More recently, heterogeneous Pt-Re catalysts have been suggested in the long-standing issue of reducing carboxylic acids and their derivates; a task that is conventionally associated with stoichiometric reagents (e.g. $LiAlH_4$) or copper chromite catalysts in harsh conditions (up to 300 bar and 400 °C).[10,11] For example, a group around Hardacre[11-13] has employed incipient wetness impregnation of Pt and Re on TiO_2 to obtain catalysts for the reduction of *N*-methyl-2-pyrrolidone in hexane (typically 120 °C, 20 bar). While the sequence of impregnation was of limited importance for catalyst activity, close interaction of both metals on the final catalyst was deemed essential. This was rationalized by DFT studies, showing C=O bond fission and subsequent hydrogenation of the resulting ad-species at the kink of a rhenium oxide top layer positioned on metallic platinum.[12] The metal oxidation states and Pt-Re electronic interactions were, however, not subject of experimental investigation. Other authors[14] have highlighted the

importance of the Pt-Re impregnation sequence in the preparation of Pt-Re/TiO_2 and Pt-Re/C above other factors. The respective synthesis consists of an initial deposition of NH_4ReO_4 followed by thermal decomposition and Pt impregnation. Consequently, a thin layer of rhenium oxides (ReO_x) covers the TiO_2 surface, thus causing reduced Pt particle size and good Pt-Re interaction. Centers of Pt and ReO_x may then allow for heterolytic H_2 dissociation, with the ensuing attack of Pt-bound hydrides on the carbonyl function of the substrate acid (hexanoic acid in dodecane, 130 °C, 50 bar H_2).

The DFT calculations of Burch et al.[12] suggest the bifunctional nature of Pt-Re/TiO_2 by assigning different roles to Re (C=O activation) and Pt (hydrogen activation). This seems to align with work by the group of Shimizu[15-17] on metal/Lewis acid bifunctional catalysts. These authors showed that Lewis acidic supports, first and foremost MoO_x/TiO_2 and Nb_2O_5, can enhance amide reduction over Pt via polarization of the otherwise unreactive C=O bond.[15] However, ReO_x/TiO_2 is not listed as promising Lewis acidic support and the same authors have shown that Re-loaded TiO_2 is a suitable catalyst for the reduction of carboxylic acid derivatives, even in the absence of Pt.[18, 19] The active state of the catalyst was narrowed down to a low-valent Re species (ON(Re) < 4), which can be achieved by H_2-treatment and subsequent handling in inert atmosphere. Consequently, Pt in Pt-Re/TiO_2 might act as an "initiator" that allows for the reduction of Re into an active state in catalysts less carefully treated. While it is now clear that the process of understanding Pt-Re catalysts is still ongoing, it should also be noted that very few systems[15, 20] can compete in the hydrogenation of carboxylic acid derivatives.

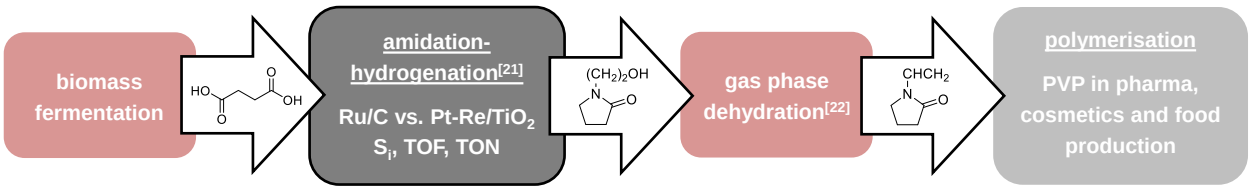

Figure 1. Value chain from biomass to polyvinylpyrrolidone (PVP) polymers with numerous applications. Catalysts for the decisive step of amidation-hydrogenation are subject of this article.

Our group has recently proposed a two-step value chain from succinic acid to *N*-vinyl-2-pyrrolidone, a valuable monomer (**Figure 1**).[21, 22] Improvements of the latter largely depend on finding a more active and selective catalyst for the reductive conversion of succinic acid and monoethanolamine into *N*-(2-hydroxyethyl)-2-pyrrolidone. While monometallic Pt catalysts were shown to be far inferior to the state-of-the-art Ru catalyst, Pt-Re/TiO_2 has significant potential. This contribution summarizes our efforts of finding and understanding an optimized Pt-Re catalyst for said hydrogenation, which is notably conducted in concentrated aqueous solution as opposed to most literature examples (0.33 mol L^{-1} octane,[18] 0.17 mol L^{-1} hexane,[12] 0.4 mol L^{-1} dodecane[14]). Consequently, the catalytic properties and structural features of Pt-Re/TiO_2 catalysts synthesized through several adapted literature procedures are presented. Comparing catalysts from co-impregnation[12] (CI), catalytic reduction[2] (CR), rhenium layer deposition[14] (LD) and strong electrostatic adsorption[23] (SEA) under otherwise identical conditions finally sheds light on the exact differences and similarities in outcome of these approaches. Moreover, the available active site hypotheses for Pt-Re hydrogenation catalysts are discussed based on results from N_2 physisorption, XRD, TPR, CO pulse chemisorption, CO-FTIR, STEM-EDX and *in-situ* XPS.

2. Experimental

2.1. Materials and Chemicals

N-(2-hydroxyethyl)-2-pyrrolidone (98 %), succinic acid (≥99 %), monoethanolamine (ACS reagent, ≥99 %), 2-MTHF (≥99 % anhydrous), 1,2-dimethoxyethane (≥99.5 % anhydrous), $NaNO_3$ (ACS reagent, ≥99 %) and NaOH (EMSURE®, ≥99 %) were sourced from Sigma Aldrich. Ethanol (absolute, 99.9 %), MTBE (99.8 %), HCl (p.a., 37 wt.%), HNO_3 (p.a., 65 wt.%) and boric acid (≥99.8 %) were obtained from ChemSolute. HF (39.5 wt.%) was obtained from Carlo Erba. All these chemicals were used as obtained and without further purification. In contrast, *N*-(2-hydroxyethyl)succinimide (abcr, ≥95 %) was dissolved in an MTBE/ethanol mixture (10/1, 55 °C reflux). The clear, hot solution was decanted and *N*-(2-hydroxyethyl)-succinimide was crystallized in a clean flask. The purified material (colorless needles) was obtained and used after washing with cold MTBE/*n*-pentane and thorough drying.

Commercial Ru/C and Pt/C reference catalysts (5 wt.% nominal loading) were obtained from Sigma Aldrich. They were tested after drying and reduction according to previously established procedures.[21] In contrast, TiO_2 supported materials were synthesized using $Pt(NH_3)_4(NO_3)_2$ (Sigma Aldrich, ≥50 wt.% Pt) and NH_4ReO_4 (ChemPur, >99.5 %) as metal precursors. The support material, anatase TiO_2 (ST6*120), was generously provided by Saint-Gobain NorPro. The shaped extrudates were ground and sieved (<180 μm) prior to use.

2.2. Catalyst Preparation

Monometallic reference materials (5 wt.% nominal metal loading) were synthesized by **wet impregnation (WI)** and are denominated as Pt/TiO_2 (WI) and Re/TiO_2 (WI). In a typical

procedure, 209 mg of $Pt(NH_3)_4(NO_3)_2$ were dissolved in 40 mL of deionized water. Subsequently, 2.0 g of pre-dried TiO_2 were slowly added, while the resulting suspension was stirred continuously. The impregnation proceeded at room temperature for 3 h. Next, the solvent was evaporated in reduced pressure and subsequent drying yielded a white powder. Thermal decomposition of the metal precursors took place in a tubular furnace at 500 °C for 3 h (2 K min^{-1}, N_2 flow). Successive reduction at 350 °C for 3 h (5 K min^{-1}, H_2 flow) led to the final catalyst.

Pt-Re/TiO_2 materials (5 wt.% Pt nominal) were synthesized by several adapted literature procedures. Wet **co-impregnation (CI)** constitutes the most straightforward case and generally follows the procedure for WI materials stated above. However, both metal precursors were jointly dissolved, which led to an apparent reduction of solubility at high Re contents.

The **catalytic reduction (CR)** approach is based on the deposition of Re on a Pt/TiO_2 (WI) parent catalyst by surface redox reactions. The following procedure is an adapted version of a previously published technique:[2] 45 mL of 0.05 M HNO_3 were added to a round-bottom flask and degassed by two successive freeze-pump-thaw cycles. Subsequently, 1.5 g of pre-dried Pt/TiO_2 (WI) was added in Ar counter current. The resulting suspension was stirred for 1 h while constantly bubbling Ar gas. This continued for another 2 h after switching to a flow of pure H_2. Meanwhile, 240 mg of NH_4ReO_4 were dissolved in 90 mL of the 0.05 M HNO_3 solution, using a separate round-bottom flask. The precursor solution was degassed following the above-mentioned procedure and then stirred for 2 h with constant Ar bubbling. Subsequently, the pre-treated precursor solution was transferred to the support suspension using a Teflon cannula. Hydrogen bubbling through the suspension continued for another hour before the flask was purged with inert atmosphere and opened. Solids were obtained after filtration, washing (200 mL

of deionized water) and drying (60 °C, 12 h). The final catalyst was directly reduced at 350 °C (3 h, 5 K min^{-1}) as is suggested by the original source.

Strong electrostatic adsorption (SEA) is limited to suitable combinations of supports, metal precursors and impregnation conditions.[24] For example, preparatory experiments showed that $Pt(NH_3)_4(NO_3)_2$ can develop a strong electrostatic interaction with the TiO_2 support (PZC ≈ 5.3) in basic solution (**Figure S1 and S2**). Thus, 209 mg of $Pt(NH_3)_4(NO_3)_2$ were dissolved in NaOH solution (150 mL, pH ≈ 12). Next, 2.0 g of pre-dried TiO_2 were slowly added and the suspension continued to stir for 1 h. The solids were obtained after filtration, washing (NaOH solution) and drying (60 °C, 12 h). Precursor decomposition and reduction followed the procedure specified for wet impregnation and yielded Pt/TiO_2 (SEA). In the absence of a suitable, negatively charged rhenium complex, Re (5 wt.% nominal) was introduced in a sequential wet impregnation step.

The **deposition of thin Re layers (LD)** has also been discussed in literature.[14] For a respective preparation, 2.0 g of TiO_2 were impregnated with NH_4ReO_4 (10 wt.% Re nominal) according to the wet impregnation procedure. This was followed by precursor decomposition in inert atmosphere (N_2 flow) as detailed in literature (10 K min^{-1}, 350 °C, 30 min). The resulting Re/TiO_2 (LD) material was then used in the sequential wet impregnation of Pt (5 wt.% nominal). After the usual drying procedures, direct reduction took place in a tubular furnace at 350 °C (5 K min^{-1}, 3 h, H_2 flow).

All bimetallic materials are denominated as $Pt\text{-}Re/TiO_2$ (x), where the abbreviation in brackets indicates the chosen preparative approach. The investigation of $Pt\text{-}Re/TiO_2$ (CR), $Pt\text{-}Re/TiO_2$ (SEA) and $Pt\text{-}Re/TiO_2$ (LD) is limited to one material each and respective rhenium loadings are defined by the given procedures (see also **Table 1**). In contrast, several co-impregnation catalysts

(Pt-(y)Re/TiO_2 (CI)) were synthesized for an exemplary investigation on the impact of the nominal rhenium loading (y) on catalytic performance. Further characterization was limited to the best-performer of this series (y = 5 wt.%, Re:Pt =1.25), which is referenced as Pt-Re/TiO_2 (CI) for brevity. All materials were stored in Argon atmosphere. However, no special techniques were employed to avoid air contact directly prior to catalytic testing (e.g., weighing).

Table 1: Physical properties of Pt-Re/TiO_2 (x) catalysts and reference materials.

Name	w(Pt) nom.[a] [wt.%]	w(Pt) exp.[b] [wt.%]	w(Re) nom.[a] [wt.%]	w(Re) exp.[b] [wt.%]	Re:Pt [mol mol^{-1}]	$SSA_{BET.}$[c] [m^2 g^{-1}]	V_{pore}[c] [ml g^{-1}]
TiO_2 (anatase)	-	-	-	-	-	162	0.40
Pt/TiO_2 (WI)	5	3.96	0	-	-	120	0.30
Pt/TiO_2 (SEA)	<5	2.40	0	-	-	83	0.33
Re/TiO_2 (WI)	0	-	5	4.62	-	134	0.35
Re/TiO_2 (LD)	0	-	10	10.4	-	124	0.32
Pt-Re/TiO_2 (CR)	5	4.42	-	0.68	0.16	120	0.33
Pt-Re/TiO_2 (CI)	5	4.25	5	5.06	1.25	114	0.31
Pt-Re/TiO_2 (SEA)	<5	2.43	5	5.00	2.16	85	0.28
Pt-Re/TiO_2 (LD)	5	3.92	10	10.1	2.70	121	0.31
spent Pt-Re/TiO_2 (LD)[d]	<5	3.94	<10	8.14	2.16	-	-

[a] nominal loading; [b] determined by ICP-OES after chemical digestion; [c] determined from N_2 physisorption isotherms; [d] after 5 use cycles (batch), Figure 4.

2.3. Catalytic Test Experiments

Batch experiments were conducted in 50 mL stainless steel autoclaves with glass inlays to protect against corrosion.[21] Typically, 37.5 mg of catalyst were added to 1.82 g of *N*-(2-hydroxyethyl)succinimid and 1.96 g of deionized water. The sealed autoclave was then purged three times with H_2, before raising the pressure to 150 bar. Subsequently, the reaction

proceeded for 6 h (150 °C, 750 rpm) before the autoclave was quenched in ice. The vessel was depressurized and opened. Next, solids were removed by filtration (polyamide syringe filter) and the clear liquid was analyzed by HPLC (Organic Acid Resin column, Chromatography Services) using a refractive index detector. In the case of recycle experiments, the reaction suspension was filtered through a polycarbonate membrane and the filter cake was washed with 60 mL of deionized water. The catalyst was reused after drying (vacuum, 60 °C) without additional heat treatments, such as reduction. Moreover, the batch size of recycle experiments was adjusted to 50 mg of catalyst to allow for easier handling and reduced relative losses in catalyst mass.

Tests in continuous operation were performed on a dedicated Parr autoclave setup (Hastelloy) equipped with a gas aspiration stirrer (1200 rpm). For a typical experiment, the autoclave was loaded with 2.0 g of catalyst powder, sealed, and purged with argon. Subsequently, hydrogen (70 bar, 200 mL min^{-1}) was admitted, and the temperature was slowly ramped to 200 °C. The liquid-providing HPLC pump was started (0.5 ml min^{-1}) at the beginning of the heating period, thus slowly filling the available liquid volume (≈ 60 mL). Surplus solution led to an output flow through a retaining frit, which was sampled for HPLC analysis (see batch experiments). Integral input and output flow rates were in good agreement. As opposed to batch experiments, the CSTR was operated with a stock solution of succinic acid (333 g, ca. 17 wt.% or 1.6 mol L^{-1}), monoethanolamine (173 g) and deionized water (1494 g). Due to the focus on hydrogenation activity (as opposed to e.g. amide formation) in CSTR and batch experiments, the following definitions are implemented (1-6). Productivities and TOFs in batch experiments are based on conversion levels below 40 %.

$$X = 1 - \frac{\sum_{i=\text{not reduced}} n_i}{n_{\text{substrate}(t=0)}} \qquad (1)$$

(thus, excludes non-catalytic, thermal equilibrium reactions)

$$Y_i = \frac{n_i}{n_{substrate(t=0)}} \tag{2}$$

$$S_i = \frac{n_i}{n_{substrate(t=0)} \cdot X} \tag{3}$$

$$\text{Productivity} = \frac{X \cdot n_{substrate(t=0)}}{n_{Me} \cdot t_{batch}} = \frac{X \cdot \dot{n}_{substrate,in}}{n_{Me}}; Me = Pt, Re, Ru \tag{4}$$

$$TON = \sum_j \left(\frac{X_j \cdot \dot{n}_{substrate,in} \cdot \Delta t_j}{n_{Pt}} \right) \tag{5}$$

(where j refers to a measurement interval of the CSTR experiment)

$$TOF = \frac{X \cdot n_{substrate(t=0)}}{n_{CO,chemisorb.} \cdot t_{batch}} \tag{6}$$

2.4. Characterization Techniques

N_2 physisorption was conducted on a Quadrasorb SI (Quantachrome). Prior to analysis, 0.2 g of powdered sample were degassed in high vacuum (250 °C, 2 h). The specific surface area (SSA) of samples was determined by the Brunauer-Emmet-Teller (BET) method applied to measurements at p/p_0 = 0.05-0.25 (adsorption branch). For elemental analysis by **ICP-OES** 20 mg of finely ground catalyst powder were dissolved in a mixture of 1 mL deionized H_2O, 4 mL HNO_3 (65 wt.%), 3.5 mL HCl (37 wt.%) and 1.5 mL HF (39.5 wt.%) using a microwave digestion vessel (10 K min^{-1}, 220 °C, 30 min). Once the liquid had cooled down, 30 mL of boric acid solution (4 wt.%) were added, followed by another heat treatment (10 K min^{-1}, 170 °C, 10 min) and, ultimately, spectrometric analysis. Powder X-ray diffraction (**XRD**) patterns were recorded on a Bruker D2 Phaser (Bragg-Brentano geometry) in ambient atmosphere using Cu Kα radiation. Reflexes were recorded at $15° < 2\Theta < 90°$ and match database entries for anatase TiO_2 (COD entry 9008214) and cubic Pt (COD entry 4334349). High-angle annular dark-field

scanning transmission electron microscopy (**HAADF-STEM**) imaging and STEM energy-dispersive X-ray spectroscopy (**STEM-EDX**) experiments with bimetallic catalysts were performed on a FEI Titan electron microscope operated at 200 kV acceleration voltage, equipped with an aberration corrector for the probe-forming lens and a "Super-X" EDX detector. HAADF-STEM imaging of monometallic samples was performed on a FEI Tecnai F20 electron microscope operated at 200kV. In both cases, particle size distributions were determined using the Fiji software package and several images from different regions of the sample. Thus, hundreds of particles were evaluated for statistical soundness of the results. Particle size distributions are given in terms of area-equivalent diameters. Temperature-programmed reduction (**TPR**) experiments were conducted on 60 mg of powdered catalyst filled into the U-shaped flow reactor of a Micromeritics AutoChem 2950 HP. Each sample was subjected to mild oxidation (10 K min^{-1}, 100 °C, 30 min) in 5% O_2/He (50 mL min^{-1}) and then dried (10 K min^{-1}, 300 °C, 60 min) in flowing He (50 mL min^{-1}). Subsequently, the oven was cooled to -50 °C using first air and then liquid N_2. H_2 consumption from 5% H_2/Ar (50 mL min^{-1}) was measured during heatup (10 K min^{-1}) to 350 °C. Moisture was removed from the reactor effluent using a cold trap filled with an iso-propanol slurry (≈ -80 °C). **CO pulse chemisorption** was performed on the same setup, using 60 mg of fresh sample. Pre-treatment consisted of drying (10 K min^{-1}, 300 °C, 1 h) in He (50 mL min^{-1}), reduction (10 K min^{-1}, 200 °C, 30 min) in 5% H_2/Ar (50 mL min^{-1}) and subsequent purging of adsorbates (10 K min^{-1}, 200 °C, 1 h) in He (50 mL min^{-1}). CO adsorption was carried out in up to 15 pulses at 35 °C. CO adsorption was also followed by Fourier-transform infrared spectroscopy (**FTIR**) on a Bruker Vertex70 spectrometer (64 scans at a resolution of 4 cm^{-1}). The respective setup and sample preparation have been described elsewhere.[22] Catalyst pellets were introduced into the flow-type

transmission cell and subjected to the same pre-treatment steps applied in pulse chemisorption. Backgrounds of the pure, reduced samples were then taken at 40 °C and 150 °C. They were employed in the collection of all subsequent CO-FTIR spectra. At 40 °C, a mixture of 50 % CO/He (10 mL min^{-1}) was flown through the cell for 5 min, after which the inlet and outlet were closed to allow for equilibration of the adsorption process. The purging and desorption of surplus CO occurred in He flow (100 mL min^{-1}), first at 40 °C and later at 150 °C. The reported spectra are those collected at the end (30 min) of each purging step, when absorption bands were stable. Unless indicated otherwise, spectra are normalized to the total area of the CO bands between 1700 and 2300 cm^{-1}. This is to focus on the distinction of different adsorption sites, whereas the total amount of adsorbed CO will be compared using pulse chemisorption. X-ray photoelectron spectroscopy (**XPS**) measurements were performed with a spectrometer from SPECS GmbH equipped with a PHOIBOS 150 1D-DLD hemispherical energy analyzer. The monochromatized Al Kα X-ray source (E = 1486.6 eV) was operated at 15 kV and 200 W. For the narrow scans, a pass energy of 20 eV was applied. The medium area mode was used as lens mode. The base pressure during the experiment in the analysis chamber was $5x10^{-10}$ mbar. To account for charging effects, all spectra were referred to the Si 2p signal (103.3 eV) of a SiO_2 reference physically mixed with the investigated material. Reduction experiments were conducted in a preparation chamber attached to the main spectrometer. The samples were heated to 150 °C and reduction was performed in 10 % H_2/N_2 for 1 h. After cooling, the samples were transferred into the analysis chamber for spectroscopy. The program CasaXPS Version 2.3.22PR1.0 was used for data evaluation. A symmetric profile function, GL(30), was used for fitting contributions from different Re oxidation states. The full-width-half-maximum parameter (FWHM) was constrained between 0 and 2 eV. The binding energies (BE) of diverse Re species

($4f_{7/2}$ contributions) were constrained to 46-45 eV (Re^{7+}), 43.8-42.8 eV (Re^{6+}) and 42.5-41.5 eV (Re^{4+}).

3. Results and Discussion

3.1. Catalyst Testing

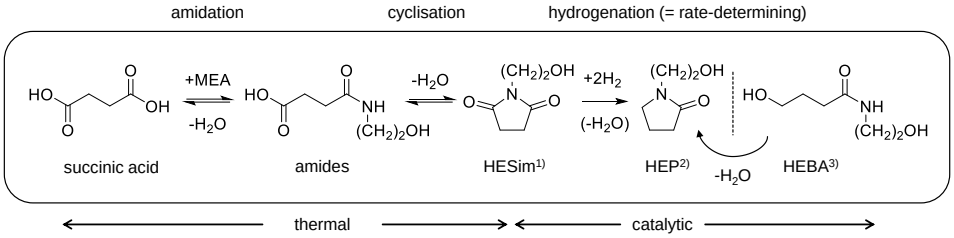

Scheme 1. Reaction network of succinic acid conversion with monoethanolamine (MEA) and H_2. [1)]*N*-(2-hydroxyethyl)succinimide; [2)]*N*-(2-hydroxyethyl)-2-pyrrolidone; [3)]*N*-(2-hydroxyethyl)-4-hydroxybutanamide;

A kinetic analysis of the reductive transformation of succinic acid with monoethanolamine (MEA) and H_2 on Ru/C has been presented previously.[21] Consequently, the reaction can be described as a sequence of fast, thermal (amidation, cyclisation) and slow, catalytic (hydrogenation) processes (**Scheme 1**). Since similar observations are made with Pt-Re/TiO_2 (**Figure S3**), catalysts can be screened in the reduction of *N*-(2-hydroxyethyl)succinimide (HESim) to *N*-(2-hydroxyethyl)-2-pyrrolidone (HEP) as a simplified model reaction. At low conversion, *N*-(2-hydroxyethyl)-4-hydroxybutanamide (HEBA) appears as the main by-product. This can be traced back to a balance between C-N vs. C-O hydrogenolysis, which is an important selectivity feature in general amide reductions.[10] The ratio S(HEBA)/S(HEP) is thus given next to catalyst productivity in subsequent screening results. However, in the special context at hand, HEBA has value as a product since it undergoes intramolecular condensation to HEP at high temperature (≥200 °C).[25]

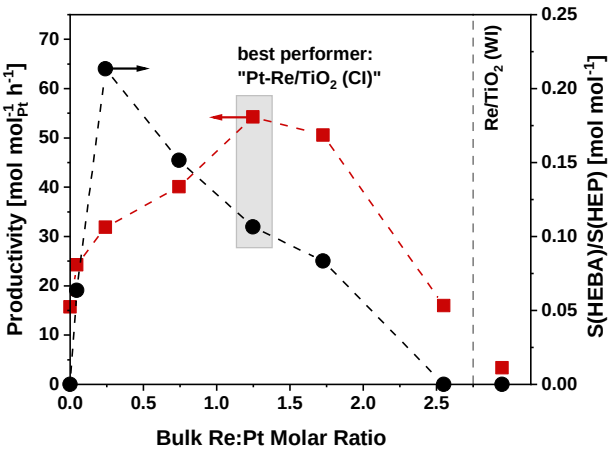

Figure 2. Comparison of the catalytic performance of Pt-(y)Re/TiO_2 (CI) in imide reduction as a function of Re:Pt ratio. A pure Re/TiO_2 (WI) material (productivity per mol_{Re}) is given for reference. Productivity (red squares) and selectivity ratio (black circles). (Conditions: 150 °C, 150 bar H_2, 6 h, 750 rpm, 37.5 mg catalyst)

The effect of Re on catalyst performance was first investigated for a set of Pt-(y)Re/TiO_2 catalysts prepared by co-impregnation (CI). Respective results (**Figure 2**) show a volcano-shaped productivity trend as a function of the material's Re:Pt ratio. Similar observations have been made for the Ir-Re system[23] and are generally indicative of synergistic behavior. Selectivity-wise, Pt-(y)Re/TiO_2 (CI) materials catalyze C-N hydrogenolysis to some extent, whereas no HEBA was formed for either of the monometallic references (Pt/TiO_2 (WI) and Re/TiO_2 (WI)). While this adds to the evidence of a new active site structure comprising both metals, it is notable that the maxima of selectivity and activity curves in Figure 2 do not coincide. It is thus likely that the exact behavior of Pt-Re/TiO_2 in catalysis is modulated by (local) composition. For example, a 1.25:1 molar ratio of Re:Pt offers a manifold increase in catalyst activity (vs. Pt/TiO_2 (WI)) at decent HEP selectivity and will thus be used as representative of the CI catalyst class in subsequent sections (briefly, Pt-Re/TiO_2 (CI)).

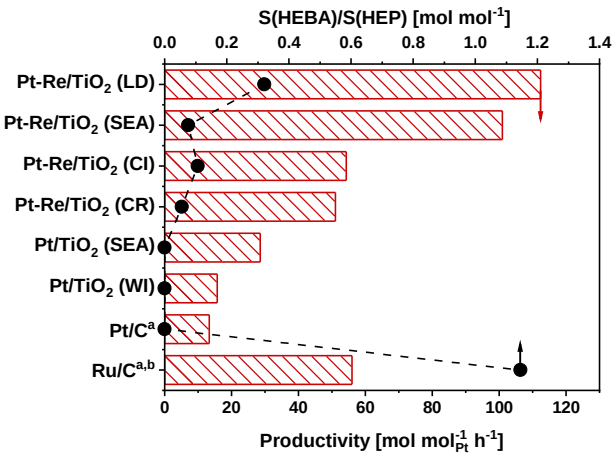

Figure 3. Comparison of several Pt-Re/TiO_2 (x) materials and reference catalysts in imide reduction. Productivity (red bars) and selectivity ratio (black circles). [a] commercial materials; [b] productivity per mol Ru; (Conditions: 150 °C, 150 bar H_2, 6 h, 750 rpm, 37.5 mg catalyst)

Further analysis was dedicated to the study of several synthesis strategies, which were previously proposed to enhance Pt-Re interaction and thus beneficially affect catalyst properties. In detail, strong electrostatic adsorption (SEA), catalytic reduction (CR) and rhenium layer deposition (LD) each led to one material with a preparation-specific Re:Pt ratio (Table 1). Taking monometallic reference materials into account, the corresponding productivity varied in the order Pt-Re/TiO_2 (LD) > Pt-Re/TiO_2 (SEA) > Ru/C (benchmark) ≈ Pt-Re/TiO_2 (CI) ≈ Pt-Re/TiO_2 (CR) > Pt/TiO_2 (WI) (**Figure 3**). Especially the high productivity of the layer deposition catalyst is surprising in that a comparable metal ratio (Re:Pt ≈ 2.2) led to inferior results in the series of CI catalysts (Figure 2). While an in-depth discussion will follow at a later stage, this serves as initial evidence of a strong impact of the preparation strategy on the catalyst structure. Selectivity-wise, all Pt-based catalysts perform better than the previously established Ru/C material.[21] However, there are differences within the presented materials and Pt-Re/TiO_2 (LD) shows the highest tendency towards C-N bond fission. As detailed above, this is of reduced importance for HESim

reduction, wherefore the Pt-Re/TiO_2 (LD) material should still be most effective in this context. However, the second most active catalyst (Pt-Re/TiO_2 (SEA)) leads to almost exclusive C-O bond cleavage and may thus merit future interest in the hydrogenation of amide substrates.

While productivities were determined at low conversion, the suitability of the Pt-Re/TiO_2 (LD) catalyst is underlined by high conversion experiments (**Table S1**), which yielded a maximum of Y(HEP) = 83 mol.%. This exceeds the performance of the commercial Ru/C benchmark (71 mol.%) and thus suggests the suppression of side-reactions over Pt-Re/TiO_2 (LD). These include HEP reduction and oligomer formation,[25] both of which are further discussed in the supplementary.

3.2. Heterogeneous Nature and Stability of the Catalyst

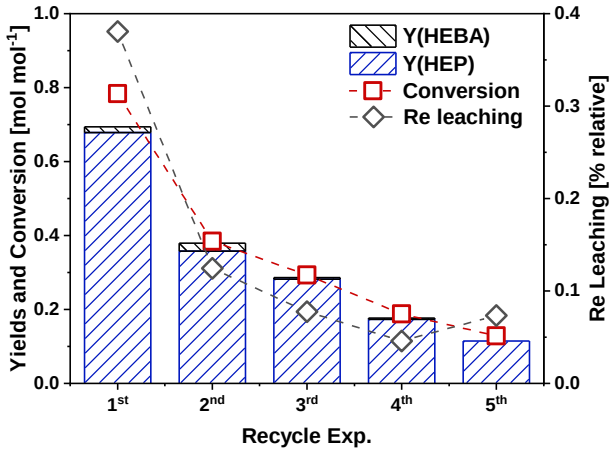

Figure 4. Batch recycling of Pt-Re/TiO_2 (LD). Dry catalyst masses were: 50.0, 47.9, 46.3, 43.5, and 41.6 mg. (Conditions: 200 °C, 150 bar H_2, 6 h, 750 rpm, recipe scaled to 50 mg of catalyst)

Given its good performance in HESim reduction, the heterogeneous nature of the Pt-Re/TiO_2 (LD) catalyst was investigated by means of hot filtration (**Figure S4**). The removal of solids from the reaction mixture after 3 h under typical conditions prevented subsequent substrate

conversion. It is therefore clear that the catalyst's reduction activity derives from species localized on the TiO_2 surface. Yet, batch recycling (**Figure 4**) was less successful, which is in line with earlier reports.[12] Similar activity loss in literature systems was attributed to the effect of cycling the catalyst between reducing and oxidizing (ambient) atmospheres.[13, 26] In this context, the use of water as solvent should be especially problematic as it likely enhances Re oxidation and leaching.[27] Accordingly, omission of the washing step in a typical recycling procedure led to a reduced loss in catalyst activity, which however still exceeded the loss in catalyst mass (not shown).

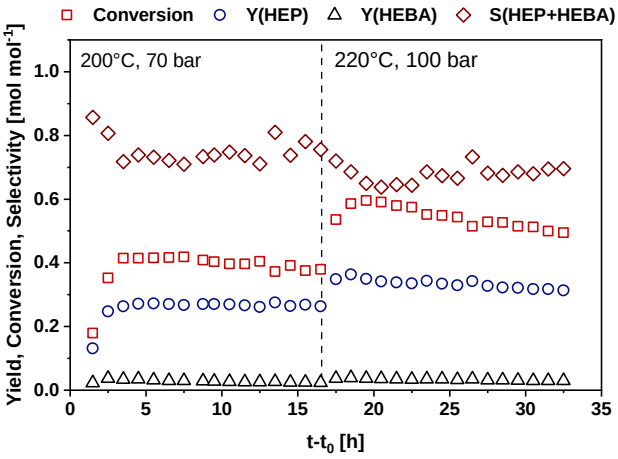

Figure 5. Results from slurry CSTR operation with the Pt-Re/TiO_2 (LD) catalyst. (Conditions: 200-220 °C, 70-100 bar H_2, $\tau_{hyd.} \approx 2$ h, Q = 0.5 ml min^{-1}, $c_{0,substrate} \approx 1.6$ mol L^{-1}, 1200 rpm, 2.0 g catalyst)

In another attempt to stabilize the bimetallic catalyst, the reaction was transferred to a CSTR setup (**Figure 5**). Being kept under reducing atmosphere, Pt-Re/TiO_2 (LD) operated with good stability for 17 h. The difference between the highest and lowest values of Y(HEP) was about 1 mol.% during that period. Slight increases in temperature and pressure boosted Y(HEP) in the second half of the CSTR run, however at the cost of selectivity. Consequently, products from

excessive reduction, such as *N*-methyl- and *N*-ethyl-2-pyrrolidone, were obtained (detailed composition: **Table S2**). In addition, slight deactivation became visible under these conditions. Yet, the catalyst maintained substantial activity after 32 h of operation (TON ≈ 1350 mol mol^{-1}_{Pt}).

Table 2: Comparison of Pt-Re/TiO_2 (LD) catalyst productivity with literature-reported systems. For a simplified comparison, nominal metal contents (wt.%) are given in brackets.

Catalyst	Substrate	Conditions	Productivity[a] [mol mol^{-1}_{Pt} h^{-1}]	Source
(5)Pt-(10)Re/TiO_2 (LD)	HESim	150 °C, 150 bar H_2	112	This study
	HESim	150 °C, 50bar H_2	47	
	succinic acid, MEA	200 °C, 70bar H_2	38[b]	
(4)Pt-(4)Re/TiO_2	*N*-methyl-2-pyrrolidone	120°C, 20bar H_2	13	[12]
(5)Re/TiO_2	*N,N*-dimethyl-2-phenylacetamide	200°C, 50bar H_2	6[c]	[19]
(5)Pt-MoO_x/TiO_2	*N*-acetylpiperidine	180°C, 50bar H_2	43[d]	[15]

[a] based on initial reaction rates at low conversion and total amount of metal in the catalyst, [b] CSTR operation at modest conversion, [c] related to Re instead of Pt, [d] given in the supplementary information of the listed reference.

These results indicate that Pt-Re/TiO_2 (LD) may yet find application in the production of biogenic *N*-vinyl-2-pyrrolidone via the proposed route. This is further underlined, by a comparison with literature-reported systems for the reduction of carboxylic acid derivatives (**Table 2**). While different substrates, solvents and initial concentrations render the evaluation of such data difficult, the presented set of catalyst and imide substrate yields productivities at the upper end of the range reported for literature systems. The possibility of continuous operation should further benefit industrial application. However, it is noted that the demonstrated CSTR setup is suboptimal since it operates under output conditions. The resulting accumulation of product inside the reactor leads to slower reaction and reduces selectivity (< 80%) due to overreduction. A PFR-type reactor, as implemented by Coetzee et al.,[13] should be preferred.

4. Catalyst Characterization

Given the variable performance of Pt-Re/TiO_2 (x) catalysts from different preparation techniques, it would be interesting to reveal the underlying structural features. This requires in-depth characterization, the results of which are summarized in Table 1 and subsequent sections.

4.1. Powder XRD

Powder X-ray diffraction was conducted to get a first impression of metal dispersion (**Figure 6**) in different catalysts. While distinct reflections of typical Re and ReO_x phases were absent in all samples, signals caused by crystalline Pt structures (cubic lattice: $2\Theta = 39.7°$, 46.3°, etc.) appeared to a variable extent. Thus, the presented catalysts can be clustered in two groups: Firstly, distinct Pt reflections are apparent for Pt/TiO_2 (WI) as well as for the bimetallic Pt-Re/TiO_2 (CI) and (CR) catalysts. Secondly, these Pt signals are much broader and tend to fuse with the baseline for Pt-Re/TiO_2 (LD) and (SEA) materials, indicating smaller Pt crystallites according to the Scherrer equation. Through additional contemplations of the sharp signal intensity at 39.7°, XRD suggests average Pt particle sizes in the order Pt-Re/TiO_2 (CI) > Pt-Re/TiO_2 (CR) ≈ Pt/TiO_2 (WI) > Pt-Re/TiO_2 (SEA) ≈ Pt/TiO_2 (SEA) ≈ Pt-Re/TiO_2 (LD), despite similar Pt contents. In this context, it is especially notable that a sequential impregnation of Re on Pt/TiO_2 (WI) and Pt/TiO_2 (SEA), yielding bimetallic Pt-Re/TiO_2 (CR) and (SEA) catalysts, had a minor influence the corresponding XRD patterns. In contrast, the co-impregnation of Pt and Re led to the most intense Pt reflection.

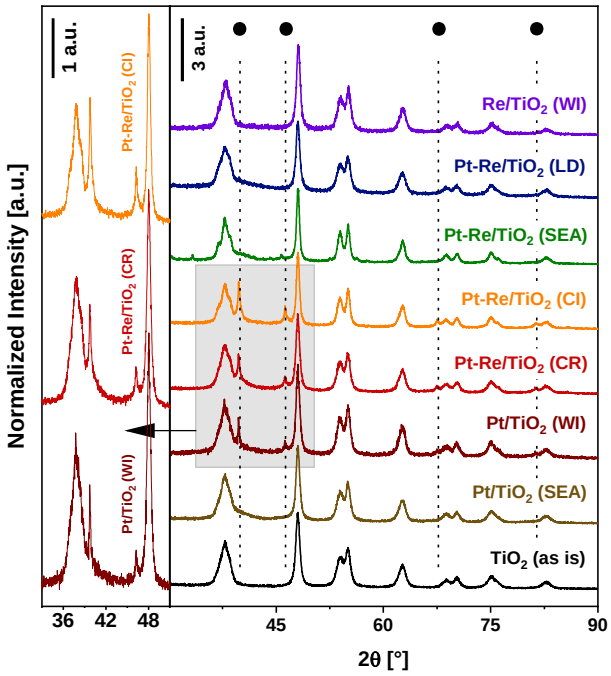

Figure 6. X-ray diffraction patterns of Pt-Re/TiO_2 (x) catalysts and reference materials. (●) reflections associated with crystalline Pt (cubic). All other peaks are assignable to the support material (anatase TiO_2).

4.2. TEM Analysis

Since XRD gives a fractional image of metal dispersion, which mostly focuses on the detection of crystallites with many repetitive planes (several nm in size), further insight was obtained through TEM analysis. In this context, it is readily apparent that pure Pt/TiO_2 catalysts from different synthesis pathways (WI and SEA) are mainly characterized by well-dispersed Pt nanoparticles (NPs) of 2-3 nm in diameter (HAADF-STEM, **Figure S6**). However, the wet impregnation (WI) catalyst additionally shows some larger (>10 nm) agglomerates, which are likely responsible for the sharp Pt reflections in the respective powder XRD pattern. It would thus appear that the SEA technique contributes to better Pt dispersion by avoiding metal

agglomeration, as has been described in literature.[24, 28] As a side effect, the achieved Pt loading is reduced (as compared to WI, Table 1) to match the uptake capacity of the support.

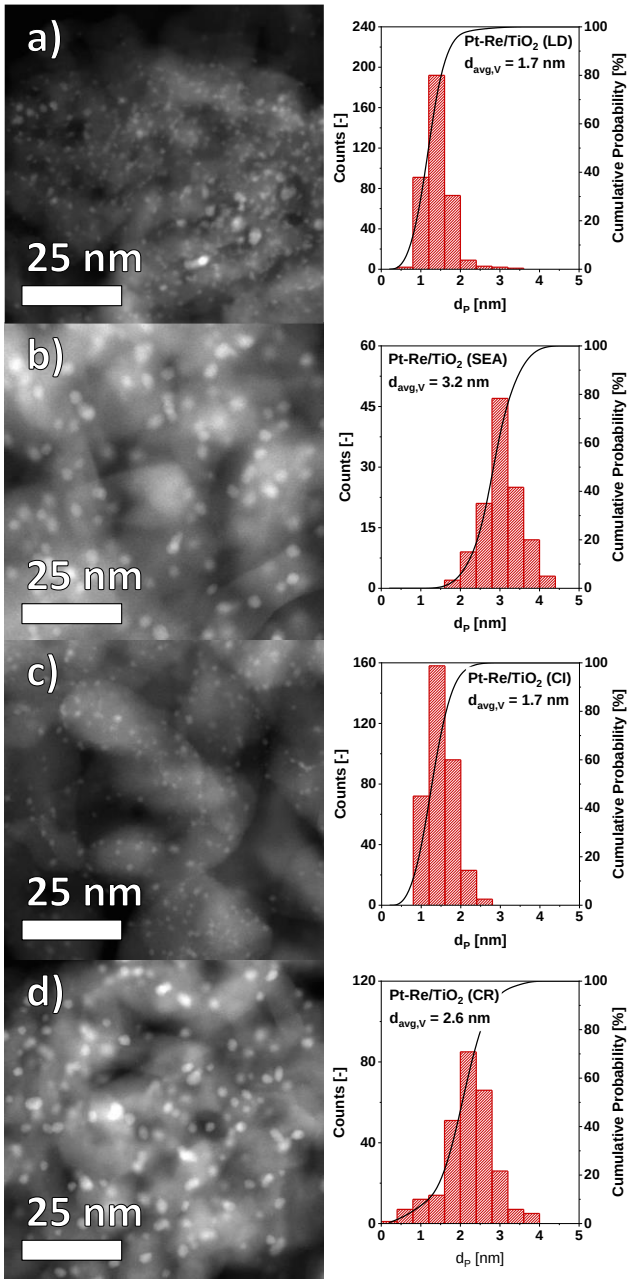

Figure 7. HAADF-STEM micrographs of Pt-Re/TiO_2 (x) catalysts. Respective nanoparticle size distributions (1-4 nm) are displayed to the right. $d_{avg,V}$ is the volume-average diameter. a) Pt-Re/TiO_2 (LD), b) Pt-Re/TiO_2 (SEA), c) Pt-Re/TiO_2 (CI) and d) Pt-Re/TiO_2 (CR).

The morphology of particles in bimetallic SEA and CR catalysts (**Figure 7b/d**) is reminiscent of the respective monometallic parents (Pt/TiO_2 (SEA) and (WI), Figure S6). This is underlined by particle size distributions reiterating the presence of NPs with sizes around 2-3 nm. In comparison, Pt-Re/TiO_2 (LD) and (CI) (Figure 7a/c) evidence smaller volume-average nanoparticle sizes ($d_{avg,V}$) despite the slightly heterogeneous appearance of the layer deposition catalyst. Due to the restriction of particle counts to the abundant small NPs (< 5 nm), this information should be combined with XRD results to give a comprehensive picture of metal dispersion on different magnification scales. While the SEA material has comparably large NPs, but no distinct Pt XRD reflections indicating metal agglomerations, the opposite is true for Pt-Re/TiO_2 (CI). Further analysis by CO-chemisorption as a bulk measure of dispersion (section 4.6) will thus be required to distinguish metal utilization on these materials. Pt-Re/TiO_2 (LD), on the other hand, displays high dispersion in XRD as well as in STEM and is thus expected to incorporate the highest density of accessible metal sites.

Moreover, EDX mappings indicate the close association of Pt and Re on the catalyst surface (**Figure 8**). While Re seems to be more evenly spread over the support than Pt, most nanoparticles show a clear enrichment in both metals. The available resolution is, however, not sufficient to derive information on particle structure (e.g. core-shell) on the nm scale. The partial spreading of Re on the metal oxide support is in line with earlier studies[14, 29, 30] and should be attributed to a strong interaction of TiO_2 and ReO_x, possibly Ti-O-Re bonds. It is most evident in the parent material (Re/TiO_2 (LD)) of Pt-Re/TiO_2 (LD), where rhenium is clearly present on nanoparticle-free areas of the support (EDX, **Figure S7**). Additionally, high-magnification STEM images of several bimetallic catalysts show evidence of small metal clusters (< 1 nm, **Figure S8**) coexisting with the previously discussed nanoparticles and metal agglomerates.

While these might also incorporate Pt atoms, their abundance apparently correlates with the Re content in different materials.

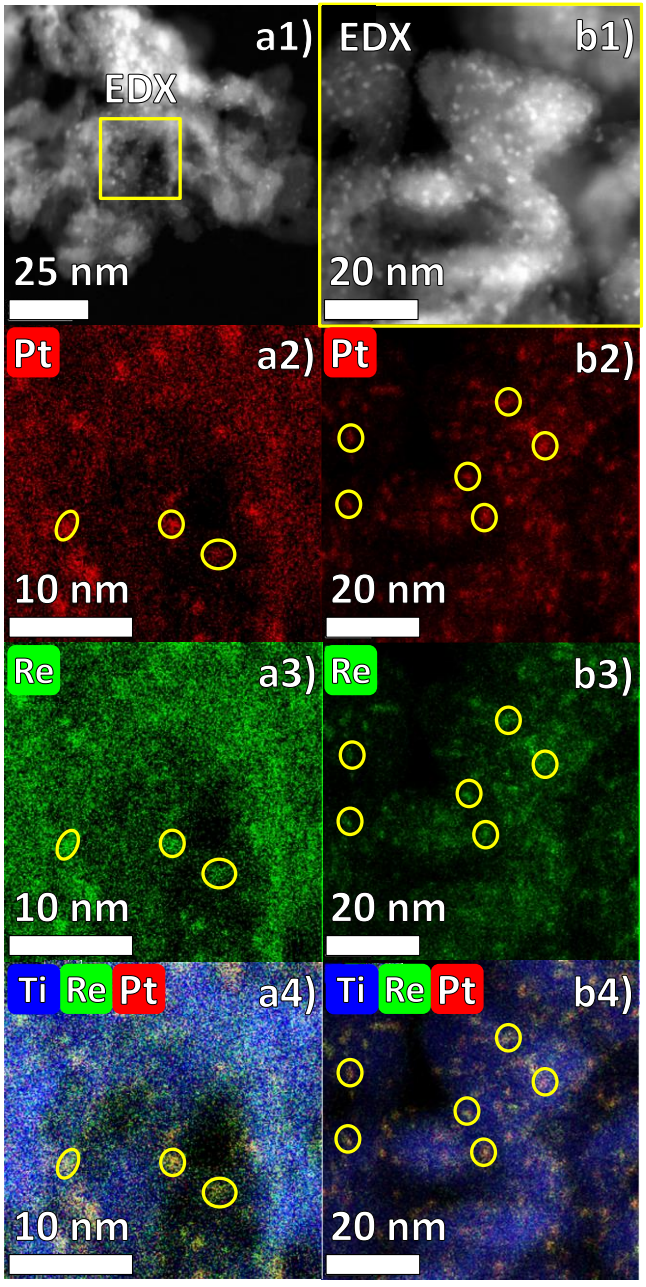

Figure 8. HAADF-STEM micrographs (a1-b2) and corresponding EDX mappings (a2-b4) of two Pt-Re/TiO_2 (x) catalysts. a) Pt-Re/TiO_2 (LD), b) Pt-Re/TiO_2 (CI). Examples of bimetallic particles are encircled in yellow.

4.3. Temperature-Programmed Reduction (TPR)

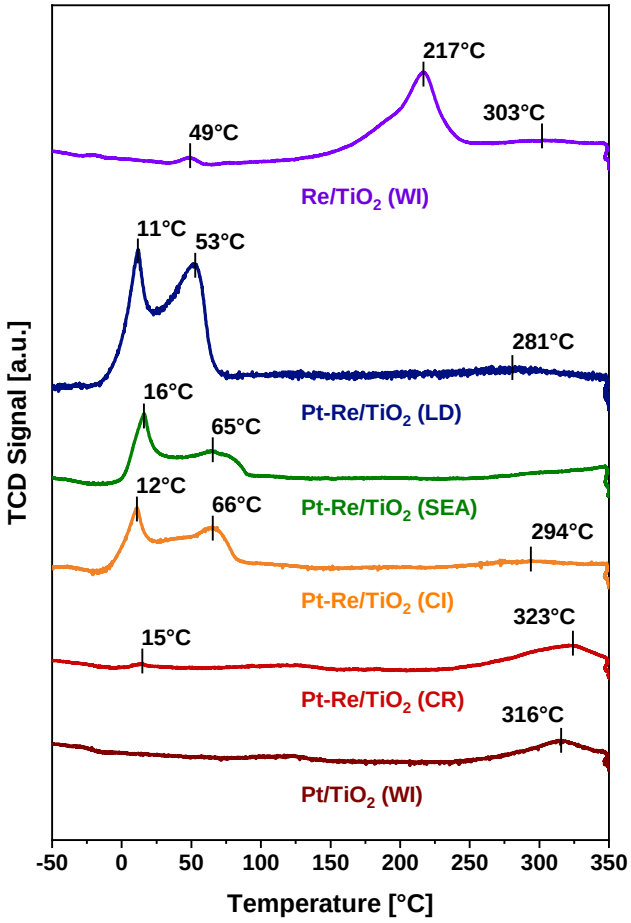

Figure 9. TPR profiles (H_2 consumption) of Pt-Re/TiO_2 (x) catalysts and reference materials. All materials were dried and oxidized in mild conditions prior to the measurement.

The association of Pt and Re on the surface of bimetallic catalysts has previously been tested by TPR.[12] In this context, it is often reported that Re reduction is enhanced by proximal Pt, possibly due to H-spillover.[3] Indeed, the main H_2 consumption feature was observed at ~220 °C for Re/TiO_2 (WI) and shifted to 10-70 °C for bimetallic materials (**Figure 9**). In contrast, only a single broad feature associated with partial support reduction (~320 °C)[12, 31] is observed for Pt/TiO_2 (WI), indicating that Pt does not directly contribute to the H_2 consumption profiles. This

is due to the specific sample preparation at hand, which likely results in Pt^0-ReO_x/TiO_2 prior to analysis. Accordingly, the absolute amount of H_2 uptake corresponding to features at 10-70 °C and 220 °C is roughly proportional to each sample's Re content (**Table 3**). Moreover, the determined stoichiometry fits the transition from Re^{7+} to Re^{4+}, suggesting partial reduction.

While complete Re reduction is indeed unlikely in the given temperature regime,[19] it should be noted that TPR is a bulk technique and thus presents an average over different Re loci. In this context, changes in the TiO_2 reduction feature (280-350 °C) for bimetallic materials underline that Re is associated with the support as well as with Pt NPs. Considering this as well as uncertainty on the catalyst state prior to TPR, further analysis is required to determine Re oxidation states in the activated material.

Table 3. Results from TPR and CO pulse chemisorption for Pt-Re/TiO_2 (x) catalysts and reference materials.

Catalyst	H_2 uptake (main red. feature[a])		CO uptake		TOF[b]
	[mmol g^{-1}_{cat}]	[mol mol^{-1}_{Re}]	[µmol g^{-1}_{cat}]	[mol mol^{-1}_{Pt}]	[h^{-1}]
Pt/TiO_2 (WI)	-	-	68	0.33	47
Re/TiO_2 (WI)	0.38	1.5	7.5	0.03[c]	184
Pt-Re/TiO_2 (CR)	0.04	1.2	31	0.14	367
Pt-Re/TiO_2 (CI)	0.42	1.5	29	0.13	411
Pt-Re/TiO_2 (SEA)	0.35	1.3	30[d]	0.24	395
Pt-Re/TiO_2 (LD)	0.77	1.4	71	0.35	318
Pt-Re/TiO_2 (LD) without reduction[e]	-	-	28	0.14	-
spent[f] Pt-Re/TiO_2 (LD)	-	-	5.5	0.03	-

[a] 10-70 °C for bimetallic materials, around 220 °C for Re/TiO_2; [b] based on productivity results from Figure 3 and CO uptake; [c] related to total moles of Re due to the absence of Pt; [d] note the reduced Pt content due to the SEA preparation technique; [e] refers to the sample pretreatment in the measurement cell; the sample had been reduced as part of the synthesis protocol; [f] after 5 use cycles (batch), Figure 4.

4.4. X-ray Photoelectron Spectroscopy (XPS)

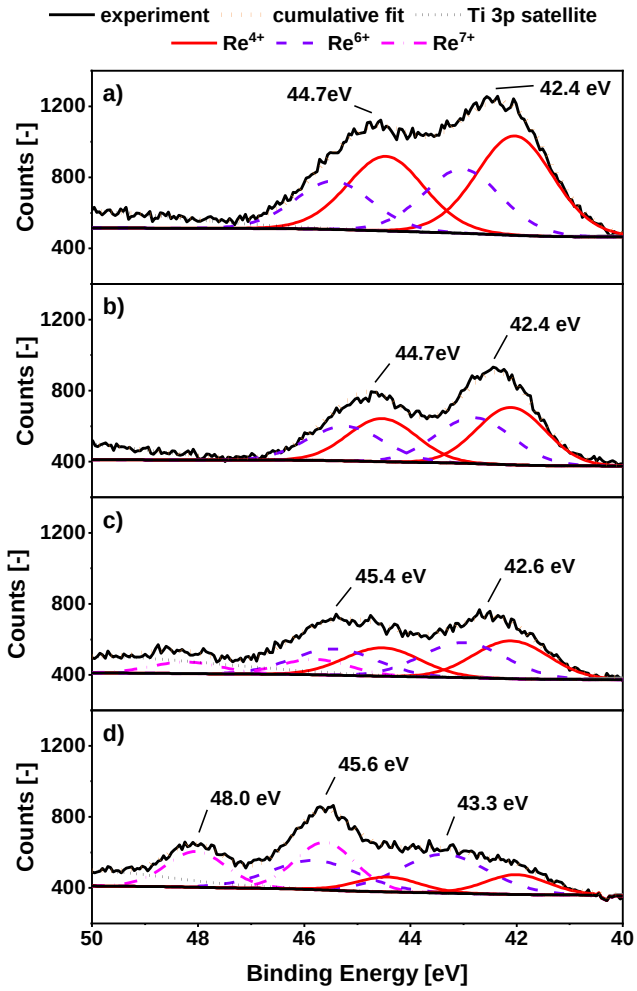

Figure 10. Re4f region of the XP spectra recorded for Pt-Re/TiO_2 (x) catalysts and reference materials after *in-situ* reduction at 150 °C. a) Pt-Re/TiO_2 (LD), b) Pt-Re/TiO_2 (SEA), c) Pt-Re/TiO_2 (CI) and d) Re/TiO_2 (WI). The signal is decomposed into the spin-orbit peaks $Re4f_{7/2}$ and $Re4f_{5/2}$ of several Re species (fitting parameters: **Table S3**). Pt-Re/TiO_2 (CR) is not evaluated due to a lack in Re signal intensity.

XPS was used to assess the oxidation states of metals in mono- and bimetallic catalysts. Prior to *in-situ* reduction, spectra of the metal 4f regions (not shown) indicate that Pt is mostly in the

metallic state, whereas Re is fully oxidized (+7) at the surface due to air contact. After reduction, the Pt signal of Pt-Re/TiO_2 (x) catalysts is well fit by a single set of $Pt4f_{7/2}$ (70.9-70.6 eV) and $Pt4f_{5/2}$ (74.2-74.0 eV) contributions, which can be represented by the symmetric GL(30) line shape, if an additional contribution from Re4s is taken into account. (**Figure S10**). In contrast, the asymmetric Pt4f contributions of Pt/TiO_2 (WI) were recorded at slightly lower binding energies (BE = 73.8 and 70.5 eV). Also, these latter signals are clearly in accordance with previous reports on the XP spectroscopy of metallic platinum surfaces.[32] On the other hand, the higher BE values for Pt in Pt-Re/TiO_2 (x) catalysts mirror literature results from Re deposition on Pt crystal planes.[32, 33] While a contribution of electronic interactions between platinum and rhenium to this phenomenon cannot be excluded, it is likely associated with evident coordination changes for surface Pt atoms (see surface core level shift). It is noted that the observed BE shift is largest for the Pt-Re/TiO_2 (LD) and Pt-Re/TiO_2 (CI) catalysts, possibly indicating a higher degree of Pt-Re association.

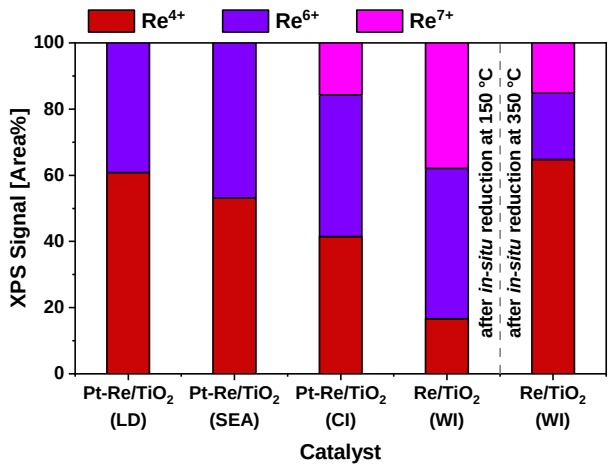

Figure 11. Distribution of Re oxidation states in Pt-Re/TiO_2 (x) catalysts and reference materials after *in-situ* reduction at 150 °C and 350 °C as determined by fitting of the XP spectra.

Analysis of the Re4f spectral region (**Figure 10**) is more complex, due to the plethora of oxidation states available to this metal.[34] However, a trend in Re4f binding energies is readily apparent from the positions of maximum photoelectron emission. The sequence of Re reduction degrees follows as Pt-Re/TiO_2 (LD) ≈ Pt-Re/TiO_2 (SEA) > Pt-Re/TiO_2 (CI) > Re/TiO_2 (WI). Additionally, peak deconvolution yields the contributions of several Re species to the overall signal (**Figure 11**), thus underlining the effect of Pt in Re reduction. In this context, it is noteworthy that the chosen reduction temperature (150 °C) is located well above the H_2 consumption maxima of bimetallic catalysts in TPR. Nevertheless, oxidized Re states prevail at the very surface of the catalyst. The same observation applies for the Re/TiO_2 (WI) reference reduced at 350 °C, which is well in line with TPR results. While the exact assignment of Re oxidation states has some uncertainty due to potential BE shifts from interactions with Pt, the recorded signal positions are clearly outside the range reported for Re^0 (40.4 eV) and Pt^0-Re^0 alloys (41.1-40.8 eV).[32,34] The existence of metallic Re after *in-situ* reduction is thus unlikely.

4.5. CO-FTIR

The surfaces of reduced catalysts were additionally probed by CO adsorption. The corresponding FTIR spectrum of Pt/TiO_2 (WI) (**Figure 12**) shows a sharp adsorption band at 2086 cm^{-1} with a broad shoulder at 2058 cm^{-1}. Based on their wavelength and earlier reports,[35-37] both bands are assigned to the linear adsorption of CO on Pt surface sites. In this context, lower wavenumbers are typically indicative of stronger adsorption on Pt atoms with high electron density and vice versa.[37] Consequently, the bands at 2086 cm^{-1} and 2058 cm^{-1} observed herein are denominated to indicate weak (Pt-Lw) and strong (Pt-Ls) CO adsorption. The corresponding surface sites may yet be harder to identify. However, the difference in Pt electron density can originate from varying coordination numbers, which would assign Pt-Lw to terrace sites, whereas Pt-Ls relates

to kinks, corners and edges.[36] Another explanation lies in the heterogeneous nature of the simple Pt WI catalyst, which evidences large Pt agglomerates next to nanoparticles. In this context, shifts in ν_{CO} have been reported as a function of metal dispersion.[38] Lastly, an additional band at 1812 cm^{-1} can be assigned to bridged CO adsorption (Pt-B).[38-40] Its intensity should thus be linked to Pt ensemble size and electron density.[40]

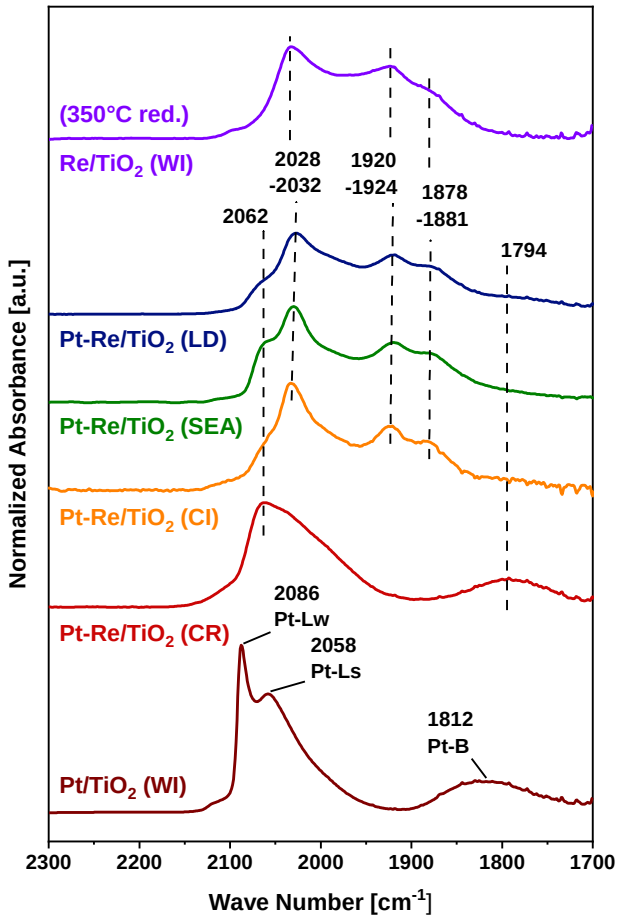

Figure 12. FTIR spectra of CO adsorbed on Pt-Re/TiO_2 (x) catalysts and monometallic references at 40 °C. Catalysts were reduced at 150 °C within the IR cell, unless stated otherwise. Spectra are area-normalized to focus on the relative contributions of IR bands.

The spectra recorded with bimetallic Pt-Re/TiO_2 (x) catalysts show additional bands around 2030, 1920 and 1880 cm^{-1}. Similar signals, which were observed with several Pt-Re/TiO_2 WGS catalysts, were previously attributed to an additional linear Pt-CO species and "a doublet [of] bridged CO[…] peaks".[41] Elsewhere,[42] these linear and bridged species have been assigned to CO adsorption on metallic Re. While linear and bridged adsorption states do exist for CO on Re, their instability at and above room temperature has been suggested.[43] Consequently, Re carbonyls can be expected to form as a function of temperature, pressure and adsorption time.[44] In this context, a configuration of Re tricarbonyl could account for all three bands identified herein.[43] Notably, Re does not have to be zero-valent in this case. While both band allocations lead to a similar conclusion, i.e. the presence of Re on the very surface of the catalyst, the latter will be assumed herein. The most important reason is that XPS results render the existence of significant amounts of Re^0 unlikely, even after *in-situ* reduction.

Interestingly, even Pt-CO bands were largely suppressed on Pt-Re/TiO_2 (LD) before *in-situ* reduction (see **Figure S11**). In combination with XPS, these results imply that rhenium oxide species – whose structure is likely affected by reduction – cover a variable fraction of the Pt surface. This is further underlined, by the presented spectra of Pt-Re/TiO_2 (x) bimetallic catalysts, which cannot be represented by a linear combination of Pt-CO (2086 cm^{-1}, 2058 cm^{-1}, 1812 cm^{-1}) and Re carbonyl (2030 cm^{-1}, 1920 cm^{-1}, 1880 cm^{-1}) bands. Pt-Re/TiO_2 (CR), which contains the lowest amount of Re, still evidences clear contributions of Pt-Ls and Pt-B to the spectrum. However, the sharp Pt-Lw band of the Pt/TiO_2 (WI) parent catalyst has disappeared in favor of a pronounced red-side tailing of the Pt-Ls band. Together with a red-shift in Pt-B, this could indicate an increase in the strength of CO adsorption. Given previous insight on the localization of Re, however, the frequency shift is likely rationalized by reduced dipole-dipole

interactions[45] due to the increased isolation of Pt-CO sites caused by Re blocking. It should be noted that partial blocking of Pt surface sites by Re has previously been discussed in the context of Re deposition by CR.[2]

The other bimetallic catalysts cannot be easily compared with Pt/TiO_2 (WI), due to the dominance of their Re carbonyl bands. However, the Pt-Lw band is clearly absent in all cases, underlining the overall red-shift of Pt-CO spectral contributions. Together with the absence of a Pt-B band, this hints towards the abundance of Re species on the surface of Pt particles. Electronic interactions between Pt and Re have also been discussed as a cause of red-shift in CO-FTIR spectra.[46] However, the respective materials contained Re in the metallic state and Re carbonyl bands were absent in CO-FTIR. Notably, this does not exclude electronic interactions of Pt and ReO_x in the case at hand. Lastly, the overall band structure for Pt-Re/TiO_2 (LD), Pt-Re/TiO_2 (SEA) and Pt-Re/TiO_2 (CI) is similar, but not identical, which hints at small modulations in surface composition. Most evidently, the Pt-Ls band (2062 cm^{-1}) of Pt-Re/TiO_2 (SEA) is comparably pronounced, which is in line with a low Pt BE shift in XPS. Both results underline a reduced coverage of Pt particles with Re species in Pt-Re/TiO_2 (SEA).

4.6. CO Pulse Chemisorption

Lastly, CO pulse chemisorption is frequently used to quantify the number of active sites in noble metal catalysts. Here, Table 3 indicates CO uptake (per mol_{Pt}) in the order Pt-Re/TiO_2 (LD) > Pt-Re/TiO_2 (SEA) > Pt-Re/TiO_2 (CI) ≈ Pt-Re/TiO_2 (CR). The same sequence has been observed in measurements of catalyst activity (Figure 3), wherefore remarkably similar TOF values were calculated for all Pt-Re/TiO_2 (x) materials. This would agree with the assumption of a shared active site structure. In contrast to bimetallic materials, Pt/TiO_2 (WI) combines high CO

uptake with a low level of productivity in HESim reduction. The resulting TOF, which is an order of magnitude below that of Pt-Re materials, shows that Re has a definitive role in constituting the active site of the bimetallic catalysts. Its function cannot be reduced to a physical promotion effect that enhances the amount of Pt surface sites.[42] On the contrary, Re species seem to block surface sites, as is most easily demonstrated with the Pt-Re/TiO_2 (CR) catalyst. Despite a Re:Pt ratio of about 0.16, half of the CO adsorption sites present in the monometallic parent (Pt/TiO_2 (WI)) have been blocked. Whilst being especially promoted by the CR synthesis strategy, this seems to be a common feature in all bimetallic materials.

In this context, it should be noted that the contribution of Re carbonyl formation to the overall CO uptake may be significantly smaller than suggested by FTIR experiments. Firstly, the extinction coefficient of Pt-CO and Re carbonyl IR bands are unknown and may prove to be of significantly different magnitude. Secondly, Re carbonyl formation has been shown to be a function of adsorption time and CO pressure,[44] both of which are significantly increased in FTIR due to experimental reasons. It is therefore less surprising that CO pulse chemisorption was previously used for the quantification of Pt sites in Pt-Re/Al_2O_3.[47]

5. Discussion

Table 4. Summary of characterization results for bimetallic Pt-Re/TiO_2 (x) catalysts.

characterization	common finding	distinctive properties
XRD	absence of Re or ReO_x reflections	clear Pt^0 reflections indicating metal agglomeration for Pt-Re/TiO_2 (CI) and Pt-Re/TiO_2 (CR)
HAADF-STEM	mainly 1-4 nm nanoparticles	$d_{avg,V}$ for NPs in Pt-Re/TiO_2 (x): LD ≈ CI < CR < SEA
EDX	joint presence of Pt and Re in nano-particles	especially for Pt-Re/TiO_2 (LD): spread of Re over TiO_2
TPR	facilitated Re reduction through Pt	variation in TPR-profile shape at T > 150 °C
in-situ XPS	metallic Pt with shifted position and attenuated intensity	degree of Re reduction in Pt-Re/TiO_2 (x): LD > SEA > CI
CO-FTIR	Re carbonyl formation and red-shift of Pt-CO bands	variable contribution of Pt-Ls and Re carbonyl bands to the spectra
CO-chemisorption	CO uptake of Pt-Re/TiO_2 (x) mostly below the Pt/TiO_2 (WI) reference	dispersion in Pt-Re/TiO_2 (x): LD > SEA > CR ≈ CI

As highlighted in the summary of characterization results (**Table 4**), Pt-Re/TiO_2 (x) materials show a set of common traits, which are independent of the chosen synthesis methods. Most notably, the TiO_2 support is covered with bimetallic Pt-Re nanoparticles in the 1-4 nm size regime. While platinum is in the metallic state, rhenium achieves partial reduction (ReO_{x-y}) after a mild treatment at 150 °C (0.1 bar H_2, XPS). In the absence of Pt, similar Re oxidation states (mostly Re^{6+}/Re^{4+}) are achieved at 350 °C, which hints at the role of hydrogen-spillover in the bimetallic system. Comparable observations have been made in literature[3, 12] and seem to be a common feature of Pt-Re catalysts. However, Sá et al.[48] suggest that Re in Pt-Re/TiO_2 catalysts can attain its metallic state (*in-situ* XANES) after gas as well as liquid phase reduction (1-20 bar H_2, 120 °C). This was not observed herein, possibly due to differences in H_2 partial pressure and catalyst preparation. Accordingly, Pt-Re alloy formation was deemed unlikely.

Further evidence on metal distribution stems from the Pt^0 XPS-signals of bimetallic catalysts (Figure S10), which are attenuated and shifted to higher BE as compared to Pt/TiO_2 (WI). This is consistent with the deposition of Re on top of Pt, causing either electronic interactions or surface core level shift.[32, 33, 46] Moreover, Re carbonyl and red-shifted Pt-CO bands were apparent in CO-FTIR. Together with the low CO uptake of most Pt-Re/TiO_2 (x) samples as compared to Pt/TiO_2 (WI), this underlines the hypothesis of platinum sites blocked by rhenium species. Indeed, this model appears necessary to reconcile different measures of dispersion from XRD, HAADF-STEM and CO-chemisorption. However, the exact structure of rhenium oxides on top of Pt is likely to depend on the experimental conditions,[49] as exemplified by the low CO uptake of Pt-Re/TiO_2 (LD) prior to *in-situ* reduction (Table 3).

The origin of Re deposition on Pt sites is evident for the Pt-Re/TiO_2 (CR) catalysts, but may be harder to explain for CI, SEA and LD synthesis strategies. Yet, it seems likely that the enhanced reduction of Re by proximal Pt is not just a consequence, but also the origin of the local association of both metals. In detail, it can be expected that the presented choice of metal precursors and thermal treatment conditions leads to the co-existence of metallic platinum and high-valent rhenium oxides in some stages of all discussed synthesis protocols. Since these rhenium species can be very mobile, even in the absence of a solvent,[34] it is likely that their reduction and deposition occurs in the vicinity of Pt^0 sites offering activated hydrogen. Given this intrinsic feature of Pt-Re/TiO_2 (x) catalysts, metal dispersion appears as prime differentiator in the characterization of the investigated materials. In this context, Pt crystallite/particle sizes (XRD/STEM) are conserved in Pt/TiO_2 parent materials upon sequential Re impregnation in the CR and SEA synthesis strategies. The joint impregnation of metal precursors (CI), on the other hand, enhances Pt agglomeration, potentially due to the intermediate formation of mixed salt

($[Pt(NH_3)_4][ReO_4]_2$) clusters on the support surface.[50] This issue is circumvented by the LD method, which initially distributes and anchors ReO_x species on the metal oxide support. An improved binding of $[Pt(NH_3)_4]^{2-}$ may then be caused by ensuing PZC changes (Figure S1).[51] Also, Pt particles may be less mobile on ReO_x/TiO_2, leading to reduced coalescence during thermal treatments.[52] This cannot be achieved by joint and a posteriori Re introduction. Schematic catalyst structures according to these findings are presented in **Figure 13**.

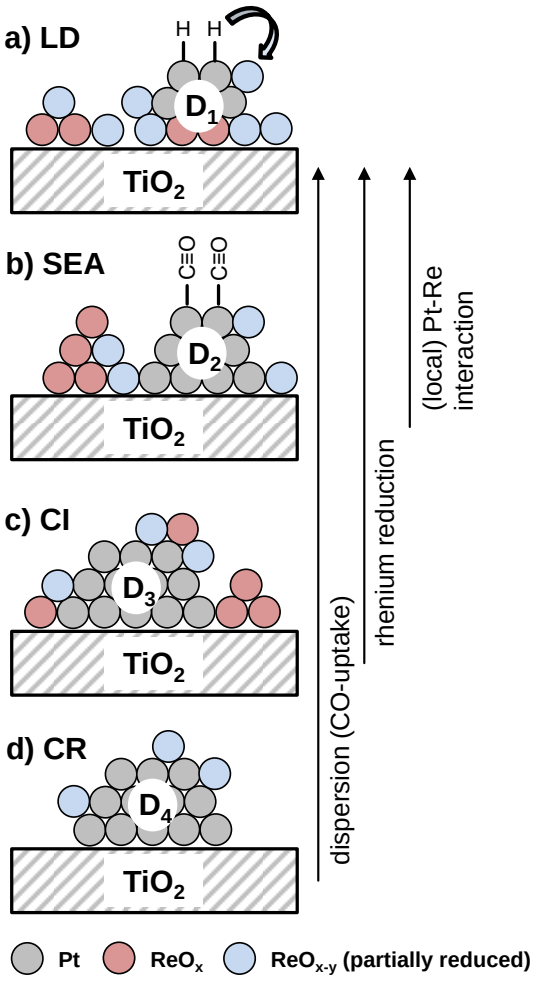

Figure 13. Comparison of the prevalent structures observed in different Pt-Re/TiO_2 (x) catalysts. a) Pt-Re/TiO_2 (LD), b) Pt-Re/TiO_2 (SEA), c) Pt-Re/TiO_2 (CI), d) Pt-Re/TiO_2 (CR). Metal dispersion follows the order $D_1 > D_2 > D_3 \approx D_4$.

The above description of Pt-Re/TiO_2 (x) materials can now be compared to literature catalysts, such as Pd-Re/SiO_2 for the hydrogenation of stearic acid.[26] The related authors found substantial Re enrichment on the catalyst surface (XPS) and no evidence of crystalline rhenium oxide (XRD). Moreover, the details of catalyst reduction had a large impact on catalytic activity, thus highlighting an optimal degree of reduction in the range of Re^{3+} and Re^{4+}. In combination with Pd^0, these species allow for substrate adsorption and H_2 dissociation. More specifically, a reaction order close to unity for $p(H_2)$ was seen as evidence of heterolytic hydrogen activation between Me^0 and Re^{n+} sites. Additional investigations on Re/TiO_2 for the hydrogenation of carboxylic acids underline the role of partially reduced rhenium.[19] For example, the oxophilic nature of ReO_{x-y} was deemed responsible for strong substrate adsorption and constant reaction rates throughout varied substrate concentrations.[18,19] Again, the reaction order regarding $p(H_2)$ was estimated near unity. Lastly, the oxophilicity of rhenium should also lead to an activation of adsorbed C=O functional groups, as demonstrated by Burch et al..[12]

Given the above and the results presented herein, Pt^0 and ReO_{x-y} jointly constitute the active site of imide reduction. Therein, the role of ReO_{x-y} is seen in substrate adsorption, which results in a lack of concentration dependence for the reaction (**Figure S12**). Since imide reduction was performed in an aqueous environment, as opposed to most of the cited literature, Pt^0 has a major role in stabilizing and regenerating partially reduced Re. This is underlined by recycling experiments, which exemplify the catalyst's instability in an oxidizing environment. Catalyst activity is then mostly a function of the density of Pt^0 sites, which tend to be associated with reducible rhenium species independent of preparation protocol. In this context, it is noted that catalyst productivity (per mol_{Pt}) also correlates with slight changes in the fraction of Re^{4+} in Pt-Re/TiO_2 (x) catalysts.

Next to the presented characterization results, the reaction order regarding p(H_2) for Pt-Re/TiO_2 (LD) was similar to Re/TiO_2[19] and Pd-Re/SiO_2[26] (**Figure S13**). While this may hint towards heterolytic H_2 activation, the potential of ReO_{x-y} for C=O activation should also be considered as origin of the enhanced Pt-Re/TiO_2 activity and further investigations in this direction are ongoing. Moreover, small differences in TOF between Pt-Re/TiO_2 (x) materials are likely accounted for by nuanced site compositions (CO-FTIR band structures and XPS). For example, a change in the Re coverage of well-dispersed Pt particles (Pt-Re/TiO_2 (SEA) vs. Pt-Re/TiO_2 (LD)) apparently has an impact on TOF and selectivity. Factors such as these deserve further investigation, e.g. by way of simplified model systems. Lastly, the reader is referred to a further discussion of the dynamics of Pt-Re bimetallic systems as well as an analysis of spent catalysts in the supplementary material (sections 12 and 13).

6. Conclusions

Amide hydrogenation using elemental H_2 and heterogeneous catalysts is a promising technology, not least in the production of nitrogen-containing chemicals from biomass. However, an understanding of the synthesis and function of the necessary bimetallic catalyst, e.g. Pt-Re/Me_xO_y, is still being developed. In this context, we presented a comparison of different synthesis strategies and the resulting Pt-Re/TiO_2 (anatase) materials in the hydrogenation of *N*-(2-hydroxyethyl)succinimide. As was previously reported, there is clear synergy of both metals in creating the active catalyst. However, productivity and selectivity also show significant variations in the series of four Pt-Re/TiO_2 catalysts obtained from different synthesis strategies.

Using in-depth characterization, mostly after *in-situ* catalyst reduction, the synthesis strategies could be connected to structural features of the resulting materials. All presented Pt-Re/TiO_2 materials show a set of comparable properties, such as partial Re reduction, blockage of Pt surface sites for CO adsorption and local association of both metals in nanoparticles as highlighted by EDX-STEM. As a result, they can be described as ReO_{x-y}-decorated Pt nanoparticles on a titania support, where the latter is modified by the spread of additional rhenium oxides. The details of the preparative approach are modulating factors, impacting on metal dispersion, Re reduction and local site composition. Consequently, different densities of active sites with slightly variable reaction behavior are obtained.

While Pt-Re/TiO_2 catalysts certainly evidence dynamic behavior due to the complex redox chemistry of Re – ranging from water-soluble, oxidized species to Re^0 in bimetallic alloys – they were successfully applied to the reduction of the substrate imide in concentrated, aqueous solution. In this context, they outperformed the previously proposed benchmark (Ru/C) in terms

of both activity and selectivity. Catalyst stability, on the other hand, is conditional on the avoidance of oxidizing atmospheres. Thus, the complete amidation-hydrogenation of succinic acid to *N*-(2-hydroxyethyl)-2-pyrrolidone has been implemented in a CSTR setup.

In the future, it would be of great interest to garner definitive information on the catalyst under reaction conditions. Consequently, the role of low-valent Re^{n+}, which is present in several recent publications may be more firmly established. In addition, the use of cheaper metals is desirable. Here, Mo and V are definitive options for the replacement of Re. However, a suitable hydrogenation metal, able to perform in comparably mild conditions, has yet to be found.

ABBREVIATIONS

XRD, X-ray diffraction; TPR, temperature-programmed reduction; FTIR, Fourier-transform infrared spectroscopy; STEM, scanning transmission electron microscopy; EDX, energy-dispersive X-ray spectroscopy; XPS, X-ray photoelectron spectroscopy; CR, catalytic reduction; DFT, density functional theory; ON, oxidation number; PVP, polyvinylpyrrolidone; CI, co-impregnation; LD, Re layer deposition; SEA, strong electrostatic adsorption; MTHF, methyl tetrahydrofuran; MTBE, methyl tert-butyl ether; WI, wet impregnation (one metal); PZC, point of zero charge; HPLC, high performance liquid chromatography; CSTR, continuous stirred tank reactor; TOF, turnover frequency; TON, turnover number; SSA, specific surface area; BET, Brunauer-Emmet-Teller method; ICP-OES, inductively coupled plasmas optical emission spectroscopy; COD, crystallography open database; HAADF, high angle annular dark field; BE, binding energy; FWHM, full width half maximum; MEA, monoethanolamine; HESim, *N*-(2-hydroxyethyl)-succinimide; HEP, *N*-(2-hydroxyethyl)-2-pyrrolidone; HEBA, *N*-(2-hydroxyethyl)-4-hydroxybutanamide; PFR, plug flow reactor; NP, nanoparticle; WGS, water-gas shift; XANES, X-ray absorption near edge structure;

AUTHOR INFORMATION

Corresponding Author: Regina Palkovits, Institut für Technische und Makromolekulare Chemie, Worringerweg 2, DE-52074 Aachen; palkovits@itmc.rwth-aachen.de

Author Contributions

The manuscript was written through contributions of all authors. All authors have given approval to the final version of the manuscript.

Funding Sources

This work was supported by the German Federal Ministry of Education and Research (BMBF) through the projects BioPyrr and BioPVP [FKZ IBÖ-03 031B0249 and 031B0487 A] in the framework of "New Products for the Bioeconomy" (Neue Produkte für die Bioökonomie). Furthermore, Mr. Haus expresses his thanks towards the German Chemical Industry Fund (Fonds der chemischen Industrie, FCI), which generously supported his PhD.

ASSOCIATED CONTENT

Electronic Supporting Information (SI). Contents: 1. Pre-Experiments for Pt-Re/TiO_2 (SEA), 2. Kinetic Analysis of Amidation-Hydrogenation over Pt-Re/TiO_2 (LD), 3. Maximum Achievable Yield, 4. Heterogeneous Nature of the Catalyst, 5. CSTR Catalyst Testing (Supplement), 6. XRD Analysis (Supplement), 7. TEM Analysis (Supplement), 8. XPS Analysis (Supplement), 9. CO-FTIR (Supplement), 10. Solvent-Effect on HESim Reduction, 11. Pressure-Dependence of HESim Hydrogenation, 12. Dynamics of Pt-Re Catalysts, 13. Characterization of Spent Catalyst. This information is available free of charge on the ACS Publications website.

ACKNOWLEDGMENT

The authors wish to acknowledge the help of Stephanie Föller and Tim Schultze in conducting the presented experiments.

REFERENCES

[1] J. Xiao and R.J. Puddephatt, Pt-Re clusters and bimetallic catalysts, Coord. Chem. Rev. 143 (1995) 457-500. 10.1016/0010-8545(94)07008-8

[2] a) C.L. Pieck, P. Marecot, C.A. Querini, J.M. Parera and J. Barbier, Influence of Pt-Re interaction on activity and selectivity of reforming catalysts, Appl. Catal., A 133 (1995) 281-292. 10.1016/0926-860X(95)00174-3 b) C.L. Pieck, P. Marecot and J. Barbier, Preparation of Pt-Re/Al_2O_3 catalysts by surface redox reactions I. Influence of operating variables on Re deposit in the presence of hydrochloric acid, Appl. Catal., A 134 (1996) 319-329. 10.1016/0926-860X(95)00237-5 c) C.L. Pieck, P. Marecot and J. Barbier, Preparation of Pt-Re/Al_2O_3 catalysts by surface redox reactions II. Influence of the acid medium on Re deposition and Pt-Re interaction, Appl. Catal., A 143 (1996) 283-298. 10.1016/0926-860X(96)00086-5

[3] R.L. Mieville, Platinum-Rhenium Interactions: A Temperature-Programmed Reduction Study, J. Catal. 87 (1984) 437-442. 10.1016/0021-9517(84)90203-3

[4] L.S. Carvalho, C.L. Pieck, M.C. Rangel, N.S. Fígoli, J.M. Grau, P. Reyes and J.M. Parera, Appl. Catal., A 269 (2004) 91-103. 10.1016/j.apcata.2004.04.004

[5] F. Hilbrig, C. Michel and G.L. Haller, A XANES-TPR Study of PtRe/Al_2O_3 Catalysts, J. Phys. Chem. 96 (1992) 9893-9899. 10.1021/j100203a058

[6] A. Ciftci, D.A.J.M. Lighthart, A.O. Sen, A.J.F. van Hoof, H. Friedrich and E.J.M. Hensen, J. Catal. 311 (2014) 88-101. 10.1016/j.jcat.2013.11.011

[7] R.W. Joyner and E.S. Shpiro, Alloying in platinum-based catalysts for gasoline reforming: A general structural proposal, Catal. Lett. 9 (1991) 239-244. 10.1007/BF00773182

[8] M. Rønning, T. Gjervan, R. Prestvik, D.G. Nicholson and A. Holmen, Influence of Pretreatment Temperature on the Bimetallic Interactions in Pt-Re/Al_2O_3 Reforming Catalysts Studied by X-Ray Absorption Spectroscopy, J. Catal. 204 (2001) 292-304. 10.1006/jcat.2001.3399

[9] S. Helfensteyn and C. Creemers, Preferential segregation to the step edges on Pt-Re catalyst particles, Surf. Sci. 507-510 (2002) 783-788. 10.1016/S0039-6028(02)01353-5

[10] A.M. Smith and R. Whyman, Review of Methods for the Catalytic Hydrogenation of Carboxamides, Chem. Rev. 114 (2014) 5477-5510. 10.1021/cr400609m

[11] H.G. Manyar, C. Paun, R. Pilus, D.W. Rooney, J.M. Thompson and C. Hardacre, Highly selective and efficient hydrogenation of carboxylic acids to alcohols using titania supported Pt catalysts, Chem. Commun. 46 (2010) 6279-6281. 10.1039/c0cc01365j

[12] R. Burch, C. Paun, X.-M. Cao, P. Crawford, P. Goodrich, C. Hardacre, P. Hu, L. McLaughlin, J. Sá and J.M. Thompson, Catalytic hydrogenation of tertiary amides at low temperatures and pressures using bimetallic Pt/Re-based catalysts, J. Catal. 283 (2011), 89-97. 10.1016/j.jcat.2011.07.007

[13] J. Coetzee, H.G. Manyar, C. Hardacre and D.J. Cole-Hamilton, The First Continuous Flow Hydrogenation of Amides to Amines, ChemCatChem 5 (2013) 2843-2847. 10.1002/cctc.201300431

[14] a) A. Suknev, V. Zaikovskii, V. Kaichev, E. Paukshtis, E. Sadovskaya and B. Bal'zhinimaev, The nature of active sites in Pt-ReO_x/TiO_2 catalysts for selective hydrogenation of carboxylic acids to alcohols, J. Energy Chem. 24 (2015) 646-654.

10.1016/j.jechem.2015.09.003 b) B.S. Bal'zhinimaev, E.A. Paukshtis, A.P. Suknev, N.V. Makolkin, Highly selective/enantioselective Pt-ReO_x/C catalyst for hydrogenation of L-malic acid at mild conditions, J. Energy Chem. 27 (2018) 903-912. 10.1016/j.jechem.2017.07.018

[15] K.-I. Shimizu, W. Onodera, A.S. Touchy, S.M.A.H. Siddiki, T. Toyao and K. Kon, Lewis Acid-Promoted Heterogeneous Platinum Catalysts for Hydrogenation of Amides to Amines, ChemistrySelect 4 (2016) 736-740. 10.1002/slct.201600088

[16] T. Toyao, S.M.A.H. Siddiki, K. Kon and K.-I. Shimizu, The Catalytic Reduction of Carboxylic Acid Derivatives and CO_2 by Metal Nanoparticles on Lewis Acidic Supports, Chem. Rec. 18 (2018), 1374-1393. 10.1002/tcr.201800061

[17] A.S. Touchy, S.M.A.H. Siddiki, K. Kon and K.-I. Shimzu, Heterogeneous Pt Catalysts for Reductive Amination of Levulinic Acid to Pyrrolidones, ACS Catal. 4 (2014) 3045-3050. 10.1021/cs500757k

[18] T. Toyao, S.M.A.H. Siddiki, A.S. Touchy, W. Onodera, K. Kon, Y. Morita, T. Kamachi, K. Yoshizawa and K.-I. Shimizu, TiO_2-supported Re as a General and Chemoselective Heterogeneous Catalyst for Hydrogenation of Carboxylic Acids to Alcohols, Chem. Eur. J. 23 (2017) 1001-1006. 10.1002/chem.201604762

[19] T. Toyao, K.W. Ting, S.M.A.H. Siddiki, A.S. Touchy, W. Onodera, Z. Maeno, H. Ariga-Miwa, Y. Kanda, K. Asakura and K.-I. Shimizu, Mechnaistic study of the selective hydrogenation of carboxylic acid derivatives over supported rhenium catalysts, Catal. Sci. Technol. 9 (2019), 5413-5424. 10.1039/c9cy01404g

[20] T. Mitsudome, K. Miyagawa, Z. Maeno, T. Mizugaki, K. Jitsukawa, J. Yamasaki, Y. Kitagawa and K. Kaneda, Mild Hydrogenation of Amides to Amines over a Platinum-Vanadium Bimetallic Catalyst, Angew. Chem. Int. Ed. 56 (2017) 9381-9385. 10.1002/anie.201704199

[21] M.O. Haus, Y. Louven and R. Palkovits, Extending the chemical product tree: a novel value chain for the production of *N*-vinyl-2-pyrrolidones from biogenic acids, Green Chem. 21 (2019) 6268-6276. 10.1039/c9gc01488h

[22] H. Krishna, M.O. Haus and R. Palkovits, Basic Silica Catalysts for the Efficient Dehydration of Biomass-Derived Compounds – Elucidating Structure-Activity Relationships for Na_2O/SiO_2-Type Materials, Appl. Catal. B 286 (2021). 10.1016/j.apcatb.2021.119933

[23] J.M. Keels, X. Chen, S. Karakalos, C. Liang, J.R. Monnier and J.R. Regalbuto, Aqueous-Phase Hydrogenation of Succinic Acid Using Bimetallic Ir-Re/C Catalysts Prepared by Strong Electrostatic Adsorption, ACS Catal. 8 (2018) 6486-6494. 10.1021/acscatal.8b01006

[24] a) M. Schreier, T.E. Feltes, M.T. Schaal and J.R. Regalbuto, The determination of oxide surface charging parameters for a predictive metal adsorption model, J. Colloid Interface Sci. 348 (2010) 571-578. 10.1016/j.jcis.2010.04.064 b) X. Hao, S. Barnes and J.R. Regalbuto, J. Catal. 279 (2011) 48-65. 10.1016/j.jcat.2010.12.021

[25] Y. Shimasaki, H. Yano, H. Sugiura and H. Kambe, Development of a New Process for *N*-Vinyl-2-pyrrolidone, Bull. Chem. Soc. Jpn. 81 (2008) 449-459. 10.1246/bcsj.81.449

[26] Y. Takeda, M. Tamura, Y. Nakagawa, K. Okumura and K. Tomishige, Characterization of Re-Pd/SiO_2 Catalysts for Hydrogenation of Stearic Acid, ACS Catal. 5 (2015) 7034-7047. 10.1021/acscatal.5b01054

[27] K. Lee, M.-E. Lee, J.-K. Kim, B. Shin and M. Choi, Single-step hydroconversion of triglycerides into biojet fuel using CO-tolerant PtRe catalysts supported on USY, J. Catal. 379 (2019) 180-190. 10.1016/j.jcat.2019.09.043

[28] S. Lambert, N. Job, L. D'Souza, M.F. Ribeiro Pereia, R. Pirard, B. Heinrichs, J.L. Figueiredo, J.-P. Pirard and J.R. Regalbuto, J. Catal. 261 (2009) 23-33. 0.1016/j.jcat.2008.10.014

[29] Z. Huang, J.R. Fryer, C. Park, D. Stirling and G. Webb, Transmission Electron Microscopy and Energy Dispersive X-Ray Spectroscopy Studies of Pt-Re/γ-Al_2O_3 Catalysts, J. Catal. 148 (1994) 478-492. 10.1006/jcat.1994.1234

[30] N. Viswanadham, R. Kamble, A. Sharma, M. Kumar and A.K. Saxena, Effect of Re on product yields and deactivation patterns of naphtha reforming catalysts, J. Mol. Catal. A Chem. 282 (2008) 74-79. 10.1016/j.molcata.2007.11.025

[31] S.S. Kim, K.H. Park and S.C. Hong, A study of the selectivity of the reverse water-gas-shift reaction over Pt/TiO_2 catalysts, Fuel Process. Technol. 108 (2013) 47-54. 10.1016/j.fuproc.2012.04.003

[32] A. Ramstad, F. Strisland, S. Raan, T. Worren, A. Borg and C. Berg, Growth and alloy formation studied by photoelectron spectroscopy and STM, Surf. Sci. 425 (1999) 57-67. 10.1016/S0039-6028(99)00185-5

[33] A.S. Duke, R.P. Galhenge, S.A. Tenney, P. Sutter and D.A. Chen, *In Situ* Studies of Carbon Monoxide Oxidation on Platinum and Platinum-Rhenium Alloy Surfaces, J. Phys. Chem. 119 (2015) 381-391. 10.1021/jp509725n

[34] M.T. Greiner, T.C.R. Rocha, B. Johnson, A. Klyushin, A. Knop-Gericke and R. Schlögl, The Oxidation of Rhenium and Identification of Rhenium Oxides During Catalytic Partial Oxidation of Ethylene: An In-Situ XPS Study, Z. Phys. Chem. 228 (2014) 521-541. 10.1515/zpch-2014-0002.

[35] K. Tanaka and J.M. White, Infrared Studies of CO Adsorption on Reduced and Oxidized Pt/TiO_2, J. Catal. 79 (1983) 81-94. 10.1016/0021-9517(83)90291-9

[36] A. Garnier, S. Sall, F. Garin, M.J. Chetcuti and C. Petit, Site effects in the adsorption of carbon monoxide on real 1.8 nm Pt nanoparticles: An Infrared investigation in time and temperature, J. Mol. Catal. A Chem. 373 (2013) 127-134. 10.1016/j.molcata.2013.02.029

[37] H.V. Thang, G. Pacchioni, L. DeRita and P. Christopher, Nature of stable single atom Pt catalysts dispersed on anatase TiO_2, J. Catal. 367 (2018) 104-114. 10.1016/j.jcat.2018.08.025

[38] J. Couble and D. Bianchi, Experimental microkinetic approach of the CO/H_2 reaction on Pt/Al_2O_3 using the Temkin formalism. 1. Competitive chemisorption between adsorbed CO and hydrogen species in the absence of reaction, J. Catal. 352 (2017) 672-685. 10.1016/j.jcat.2017.05.015

[39] S. Zafeiratos, G. Papakonstantinou, M.M. Jacksic and S.G. Neophytides, The effect of Mo oxides and TiO_2 support on the chemisorption features of linearly adsorbed CO on Pt crystallites: and infrared and photoelectron spectroscopy study, J. Catal. 232 (2005) 127-136. 10.1016/j.jcat.2005.03.003

[40] B.L. Mojet, J.T. Miller and D.C. Koningsberger, The Effect of CO Adsorption at Room Temperature on the Structure of Supported Pt Particles, J. Phys. Chem. B 103 (1999) 2724-2734. 10.1021/jp983283e

[41] Y. Sato, K. Terada, S. Hasegawa, T. Miyao and S. Naito, Mechanistic study of water-gas-shift reaction over TiO_2 supported Pt-Re and Pd-Re catalysts, Appl. Catal., A 296 (2005) 80-89. 10.1016/j.apcata.2005.08.009

[42] a) H. Iida and A. Igarashi, Difference in the reaction behavior between Pt-Re/TiO_2 (Rutile) and Pt-Re/ZrO_2 catalysts for low-temperature water gas shift reactions, Appl. Catal., A 303 (2006) 48-55. 10.1016/j.apcata.2006.01.029 b) H. Iida and A. Igarashi, Characterization of a Pt/TiO_2 (rutile) catalyst for water gas shift reaction at low-temperature, Appl. Catal., A 298 (2006) 152-160. 10.1016/j.apcata.2005.09.032

[43] F. Solymosi an T. Bánsági, CO-Induced Changes in Structure of Supported Rhenium, J. Phys. Chem. 96 (1992) 1349-1355. 10.1021/j100182a061

[44] J.A. Anderson, F.K. Chong and C.H. Rochester, IR study of CO adsorption on Pt, Re and Pt-Re/Al_2O_3 catalysts before and after coking, J. Mol. Catal. A Chem. 140 (1999) 65-80. 10.1016/S1381-1169(98)00210-6

[45] M. Scheffler, The influence of lateral interactions on the vibrational spectrum of adsorbed CO, Surf. Sci. 81 (1979) 562-570. 10.1016/0039-6028(79)90120-1

[46] A.S. Duke, K. Xie, A.J. Brandt, T.D. Maddumapatabandi, S.C. Ammal, A. Heyden, J.R. Monnier and D.A. Chen, Understanding Active Sites in the Water−Gas Shift Reaction for Pt-Re Catalysts on Titania, ACS Catal. 7 (2017) 2597-2606. 10.1021/acscatal.7b00086

[47] C.L. Pieck, C.R. Vera, J.M. Parera, G.N. Giménez, L.R. Serra, L.S. Carvalho and M.C. Rangel, Metal dispersion and catalytic activity of trimetallic Pt-Re-Sn/Al2O3 naphtha reforming catalysts, Catal. Today 107-108 (2005) 637-642. 10.1016/j.cattod.2005.07.040

[48] J. Sá, C. Kartusch, M. Makosch, C. Paun, J.A. van Bokhoven, E. Kleymenov, J. Szlachetko, M. Nachtegaal, H.G. Manyar and C. Hardacre, Evaluation of Pt and Re oxidation state in a pressurized reactor: difference in reduction between gas and liquid phase, Chem. Commun. 47 (2011), 6590-6592. 10.1039/C1CC10895F

[49] A.S. Duke, R.P. Galhenage, S.A. Tenney, S.C. Ammal, A. Heyden, P. Sutter and D.A. Chen., *In Situ* Ambient Pressure X-ray Photoelectron Spectroscopy Studies of Methanol Oxidation on Pt(111) and Pt–Re Alloys, J. Phys. Chem. C 119 (2015) 23082-23093. 10.1021/acs.jpcc.5b07625

[50] A. Nijem, S. Dery, M. Carmiel, G. Horesh, J. Garrevoet, K. Spiers, G. Falkenberg, C. Marini and E. Gross, Bimetallic Pt-Re Nanoporous Networks: Synthesis, Characterization, and Catalytic Activity, J. Phys. Chem. C 122 (2018) 24801-24808. 10.1021/acs.jpcc.8b07863

[51] X. Hao, L. Quach, J. Korah, W.A. Spiecker and J.R. Regalbuto, The control of platinum impregnation by PZC alteration of oxides and carbon, J. Mol. Catal. A Chem. 219 (2004) 97-107. 10.1016/j.molcata.2004.04.026

[52] K.G. Azzam, I.V. Babich, K. Seshan and L. Lefferts, A bifunctional catalyst for the single-stage water-gas shift reaction in fuel cell applications. Part 2. Roles of the support and promoter on catalyst activity and stability. J. Catal. 251 (2007) 163-171. 10.1016/j.jcat.2007.07.011

For Table of Contents Only